

Decentralized PV-BES Coordination Control with Improved Dynamic Performance for Islanded Plug-n-Play Dc Microgrid

Dong Li, *Student Member, IEEE*, Carl Ngai Man Ho, *Senior Member, IEEE*

Abstract— In this paper, a decentralized PV-BES coordination control method for Plug-n-Play (PnP) dc microgrid (MG) is proposed. With proposed control method, PV units can operate under dc bus voltage control when battery energy storage (BES) units are saturated due to SoC limit or charging/discharging power limit. The mode transition and power sharing are based on a communication-less manner. By bypassing communication, the MG system can become more flexible and reliable. The proposed control system contains controllers for PV converter and BES converter, respectively. The PV converter controller can achieve seamless mode transition between MPPT control and droop control. BES converter controller has a decoupled feature that a high-pass-filter (HPF) path could improve MG dynamic performance under generation-dominating mode. The BES HPF compensation overcomes the issue of poor dynamic performance under PV-dominating mode and makes the system more resistive to PV parameter variation. The Detailed design, analysis and implementation of the proposed PV-BES coordination control is provided in this paper. Simulation and experimental results have been provided to verify the concept and analytical study.

Keywords—dc microgrid, modular microgrid, decentralized control, droop control

I. INTRODUCTION

Photovoltaic (PV) generation has become a mainstream power source in the past decade. Advantages of wide distribution and zero emission have made PV generation a promising energy solution for remote areas [1]-[3]. Compared to conventional centralized power system, PV generation has a distributed characteristic, which relies on microgrid (MG) as an effective way to utilize solar energy [4]-[7]. As an integration of generation, load and energy storage, MG could constantly supply stable power and support a variety of loads, while maintaining a low upfront cost and a short leading time.

Besides conventional central-designed MG, scalable Plug-n-Play (PnP) MG has become a hot topic in both academic and industrial areas [8]-[10]. Fig. 1 shows a conceptual diagram of a scalable PnP MG. A PnP MG could further reduce the design and installation cost and allows user to grow the power network organically as demand growing [11]. Among the various types of MGs, dc MG has gained more attentions due to its reliability, efficiency, and simplicity of control, which is suitable for islanded PnP MG applications [8].

The scalable PnP MG has become a promising solution to the energy poverty problem in rural areas. To achieve high modularity and scalability in PnP MG, the key considerations

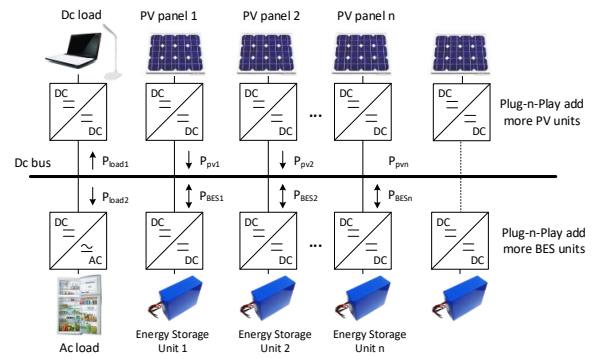


Fig. 1 Scalable Plug-n-Play microgrid.

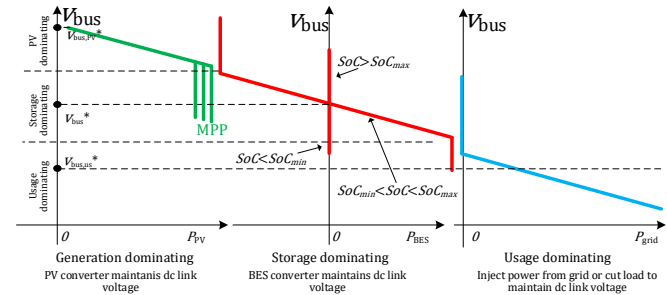


Fig. 2 Decentralized mode adaptive using dc bus signaling.

of design are different from conventional central-designed MG. Besides a highly modularized hardware structure (Full Power Processing converters for both PV and battery converters), a fully decentralized control system independent from communication should also be developed, where droop control is the most commonly used decentralized control method to achieve voltage regulation and power sharing among MG components [12].

Different from grid-tied MG systems, there is no main utility grid to support energy or stabilize voltage in islanded MG. The power balance needs to be maintained by local MG components. Usually, Battery Energy Storage (BES) systems are used to balance the power mismatch between generation and load with droop control [8]. However, a BES system cannot be available all the time due to its State-of-Charge (SoC) limit and charging/discharging power limit. Thus, it is necessary to have PV generation as bus voltage regulator when BES is saturated [13]. Thus, besides Maximum Power Point Tracking (MPPT) mode, PV converters should be able to operate under droop

control mode to enhance system capability of dc bus voltage regulation.

To achieve power sharing and mode transition at the same time without communication, literature [14] proposed a decentralized mode-adaptive control technology with dc bus signaling to achieve communication-less droop control coordination. And [15] has applied this decentralized control method to a PnP microgrid system for remote electrification. This decentralized control method could provide higher reliability, flexibility and scalability than associating with an additional central controller and a communication link. Fig. 2 shows the conceptual diagram. To better represent the droop controls used in this paper, the diagram in Fig. 2 is in a P-V plane rather than a I-V plane. When BES is available, dc bus is under BES droop control, namely storage-dominating mode. When BESs are full or at maximum charging power, dc bus voltage will rise and PV will operate in droop control mode rather than MPPT mode, namely generation-dominating mode. The vertical MPP lines represent the uncertain maximum power of PV generations. When BESs are drained or at maximum discharging power, dc bus voltage will decrease and MG will inject power from outer network or reduce load, namely usage-dominating mode. For study of islanded MG, this paper is more focused on generation-dominating mode and storage-dominating mode.

Besides mode adaption, PV generation need to be able to operate under bus voltage control mode while most of current PV products only considers MPPT control. However, the conventional droop control is usually used for BES system [16]. The performance would be deteriorated when applying to PV generation. The bus voltage regulation could become very weak under generation-dominating mode, especially at light-load condition. The PV parameters could vary a lot due to different weather conditions, which also increases the design difficulty of control system. As a result, the transient could have very large overshoot which could damage system or cause safety problems [17]. Thus, for PV generation, it is neither robust nor safe to simplify apply droop control in generation-dominating mode.

Literatures [13] and [18] have provided some solutions to solve this problem to use other control methods rather than conventional V-I droop control. Paper [13] proposed to use model predictive control to achieve both MPPT control and droop control of PV generation system. However, the mode transition relies on a switch to select mode, which reduces system robustness and the control algorithm is complicated which requires more advanced computing units. Paper [18] proposed a control method that the inner loop controls dP/dV to overcome the drawback of lacking loop gain at MPP with conventional inner PV voltage loop. However, it highly relies on accurate measurement and derivative calculation which can be expensive and is less robust towards noises. Other approaches use additional devices, e.g. [19] used super capacitors, to help voltage regulation under PV-dominating mode, which could increase cost and reduce system reliability due to the additional components.

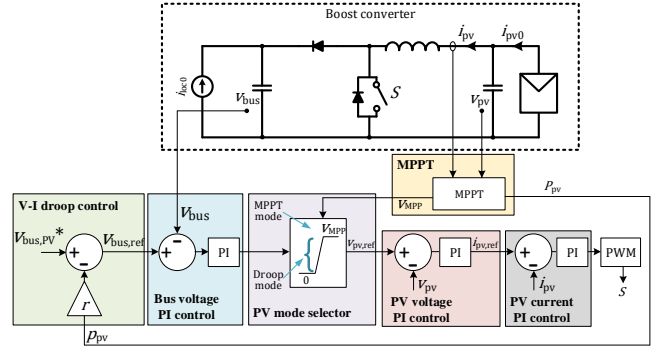


Fig. 3 Block diagram of PV converter controller with seamless mode selection.

This paper proposed a method using existing BES system to compensate the transient energy and keep the voltage regulation at an acceptable performance even under generation-dominating mode, without adding any additional component. The conventional BES controller is separated into two paths, a low-pass-filter (LPF) path and a high-pass-filter (HPF) path. The LPF path balances power at steady state and the HPF path balances power at transient. The LPF and HPF paths have separate SoC limit and charging/discharging limit. Thus, even when BES is saturated, BES can still contribute to dynamic compensation. The combined performance of two control paths are same as conventional I-V droop control. With proposed method, the microgrid can be kept stable and robust under generation-dominating mode with PV generation and without any additional cost.

The contribution of this paper:

- 1) Proposed decentralized communication-less control for PV and BES converters respectively, with seamless mode transitions, which is more robust and highly suitable for PnP MG.
- 2) Provided small signal models for PV converter under bus voltage droop control. The effect of PV parameter variation is analyzed.
- 3) Proposed a decoupled BES control method that BES can still provide dynamic compensation under PV-dominating mode which enhances voltage regulation performance under PV-dominating mode towards PV parameter variation.

The paper is organized as following: In Section II, the proposed control system for PV and BES converters are introduced, respectively. In Section III, small signal analysis of PV bus voltage control is conducted on each control loop and the overall system, the effect of PV parameter variation and proposed BES HPF compensation are studied. Section IV provides simulation and experiment results to verify the proposed coordination control. And conclusion is given in Section V.

II. PROPOSED CONTROL SYSTEM

In order to achieve PnP feature of PV and BES modules in dc microgrids, a fully decentralized control system independent from communication is proposed in this paper. The control system contains individual controllers for BES converter and PV converter, respectively. With proposed control method, control parameters of existing converters do not need any adjustment when a new PV or BES module is installed into the MG. The

robustness and fast response of dc link voltage regulation can be maintained under both storage-dominating and generation-dominating modes. The general droop coordination is based on dc bus voltage signalling as shown in Fig. 2. Detailed design is given as following.

A. Proposed PV Converter Control Method

Fig. 3 shows the proposed mode adaptive PV control diagram. There are three control loops where the inner loop controls PV output current, the middle loop controls PV terminal voltage and the outer loop is V-I droop control loop. The output of outer v_{bus} loop goes through a saturator, of which the upper limit is set to MPP voltage V_{MPP} . By setting the rated bus voltage of PV droop control, $V_{bus,PV}^*$ higher than that of BES converters, the output of v_{bus} PI controller will always be saturated to V_{MPP} , as long as the bus voltage is regulated by BES converters. When BESs are overcharged, v_{bus} will rise up higher than $v_{dp,ref}$, and, as a result, $v_{PV,ref}$ will decrease to lower than V_{MPP} . Thus the PV module will operate with reduced output power, and the seamless mode transition of PV module can be achieved. Noted that the saturation characteristic of $v_{PV,ref}$ requires an integrator in the droop control, which explains why V-I droop control is used for PV converter control rather than I-V droop control [19].

Different from a typical V-I droop controlled system, the proposed PV controller has three control loops. It requires two loops (v_{pv} loop and i_{pv} loop) to stabilize PV output power rather than a simple current loop for BES applications. And since the bandwidth of MPPT control is much slower than the PV voltage loop, in steady state, i_{pv} is equal to i_{pv0} . Thus i_{pv} , rather than i_{pv0} can be used for MPPT controller to reduce the number of current sensors. Furthermore, different from a typical V-I droop control, it is actually a V-P droop control which uses power measured on the PV panel side to replace the measured current on the dc bus side, which can further reduce the number of current sensors. For the proposed PV control system, only one current sensor in total is required.

The maximum inner loop bandwidth is limited by switching frequency, and each control loop should typically have a 5-10 times bandwidth difference with their neighbor. As a result, increased number of control loops will deteriorate the outer loop dynamic performance. The controller performance will be discussed in Section III with a small signal analysis. And the proposed BES converter controller, which will be discussed in next section, will provide dynamic compensation to help voltage regulation under PV-dominating mode to address this issue.

B. Proposed BES Converter Control Method

As mentioned above, PV droop control has a relatively poor dynamic performance on bus voltage regulation. Furthermore, the power flow of PV converter is unidirectional. As a result, at zero load condition, if BESs cannot further absorb energy, the bus voltage will be kept at the peak overshoot value due to the energy cannot be consumed. Thus, it is necessary to keep the ability of dynamic regulation of BES converters even under generation-dominating mode. Different from PV converter, BES converter does not need complicated mode transition. I-V droop control can be used. Only one current loop is used in I-V droop control. The bandwidth can be much higher than that of V-I droop control. With BES helping PV droop control, the dynamic

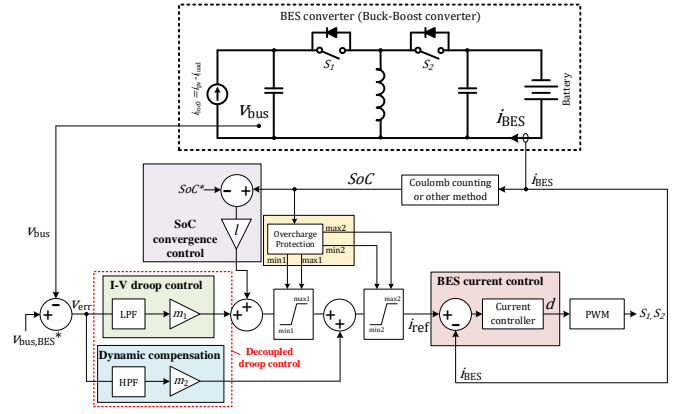


Fig. 4 Block diagram of SoC-based droop control for BES converter.

TABLE I. SATURATOR LIMITS DESIGN EXAMPLE

SoC level	Saturator on LPF path		Saturator for combined current reference	
	min1	max1	min2	max2
$SoC > 100\%$	0	5A	0	8A
$SoC > 95\%$	0	5A	-6A	8A
$30\% < SoC < 95\%$	-3A	5A	-6A	8A
$SoC < 30\%$	-3A	0	-6A	8A
$SoC > 25\%$	-3A	0	-6A	0

response can be kept at high performance under both storage-dominating mode and generation-dominating mode.

Fig. 4 shows the block diagram of proposed BES controller. The conventional I-V droop control is decoupled into two paths with a low-pass filter (LPF) and a high-pass filter (HPF). The LPF path could provide the ability of power sharing and power balance at steady state. The HPF path which is a dynamic compensation path is used to compensate transient energy. The combined performance is similar to that of conventional I-V droop control if time constant of LPF and HPF are selected same. The decoupled design has following advantages,

1) Different current limits can be put on two paths. The main power flow is determined by the LPF path. The HPF path only has minor effect on energy exchange, which will not affect BES SoC level significantly. Thus, BES dynamic compensation path can be kept active even when LPF path is saturated. Table I shows a design example of saturator limits.

2) Different droop coefficient can be applied to two paths. The LPF path can have a large m_1 value to narrow the bus voltage steady state error. The HPF path can have a relatively small m_2 value to avoid impact of noise.

For steady state analysis, the effect of HPF path can be neglected.

A SoC term is also added to the BES I-V droop control to achieve SoC self-convergence. Different from existing SoC self-convergence control that modifies droop coefficient [15][20], the proposed control adds an offset to the droop line to better fit the dc bus voltage signaling technology. Besides the conventional I-V droop term that output current is proportional to voltage error, it contains an SoC ramp term. With the additional term, the output current will slightly increase when the BES SoC level is higher than SoC^* ; the output current will slightly decrease when SoC level is lower than SoC^* . Thus, SoCs among multiple BESs can get to a convergence.

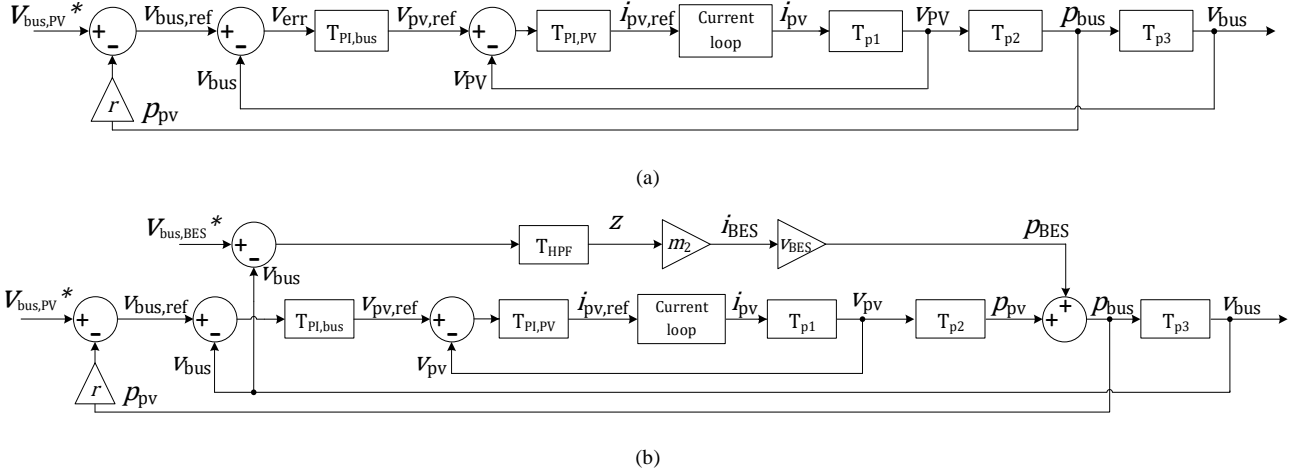


Fig. 5 Control block diagrams of v_{bus} droop control under generation-dominating mode, (a) without BES decoupled droop control, and (b) with BES decoupled control.

TABLE II. PARAMETERS FOR SMALL SIGNAL ANALYSIS

Symbol	Value	Symbol	Value
$V_{bus,BES}^*$	48 V	$V_{bus,PV}^*$	53 V
C_{bus}	660 μ F	C_{PV}	200 μ F
$k_{p,bus}$	3.5	m_1	1
$k_{i,bus}$	100	m_2	1
$k_{p,PV}$	10	t_{LPF}	0.01
$k_{i,PV}$	2	t_{HPF}	0.01
r	1/100	V_{BES}	48 V

III. SMALL SIGNAL ANALYSIS

As mentioned, with conventional V-I droop control, dc bus voltage regulation has a relatively poor dynamic performance with PV droop control due to the low control bandwidth and lack the ability of bidirectional power flow. A decoupled BES droop control strategy is proposed to improve system performance under generation-dominating mode. This section mainly studies the voltage regulation performance under generation-dominating mode with small signal analysis.

Notice that, besides the droop controller, the PV controller has a triple loop structure (PV current loop, PV voltage loop and dc bus voltage loop). Thus, the control parameters need to be carefully selected to avoid any interactions among the control loops. Bode diagrams which can clearly show the crossover frequency of each control loop, is used to show guide the design of each control loop. And for the overall system including the V-I droop controller, a state space model is derived from the transfer function models, which is more convenient to evaluate the overall system performance.

A. Transfer function models

Fig. 5 (a) shows the control block diagrams of v_{bus} droop control under generation-dominating mode without BES HPF compensation. Fig. 5 (b) shows the control block diagram that with BES HPF compensation. It can be seen that the BES HPF compensation could add a feedforward control path to the system.

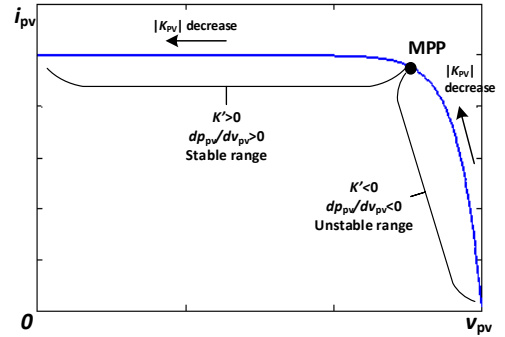


Fig. 6 PV curve showing parameters variation.

The current controller of PV converter can be achieved with hysteresis controller or PI controller with high control bandwidth. The response speed of PV current loop is much faster than that of outer loops. To simplify the study, the closed-loop transfer function of PV current loop can be regard as 1.

PV arrays has a nonlinear I-V characteristic. Usually a linearized express can be written as,

$$\tilde{i}_{PV0} = K_{PV} \tilde{v}_{PV} \quad (1)$$

where K_{PV} can be expressed as,

$$K_{PV} = \frac{N_p I_{sc,n}}{[\exp(V_{oc,n}/aV_t) - 1] a N_s V_t} \cdot \exp\left(\frac{v_{PV}}{a N_s V_t}\right) \quad (2)$$

K_{PV} is always negative and the detailed parameters for PV modeling can be found in [21][22].

By adding perturbation to v_{PV} differential equation,

$$C_{PV} \frac{d(V_{PV} + \tilde{v}_{PV})}{dt} = I_{PV0} + \tilde{i}_{PV0} - I_{PV} - \tilde{i}_{PV} \quad (3)$$

Putting (1) into (3), T_{p1} can be expressed as,

$$T_{p1} = \frac{\tilde{v}_{PV}(s)}{\tilde{i}_{PV}(s)} = \frac{1}{-C_{PV} s + K_{PV}} \quad (4)$$

By adding perturbation to p_{PV} calculation,

$$P_{PV} + \tilde{p}_{PV} = (V_{PV} + \tilde{v}_{PV}) \cdot (I_{PV} + \tilde{i}_{PV}) \quad (5)$$

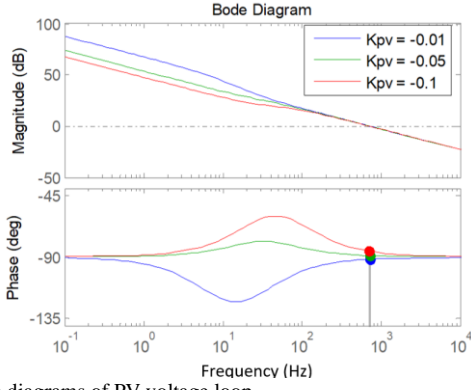


Fig. 7 Bode diagrams of PV voltage loop.

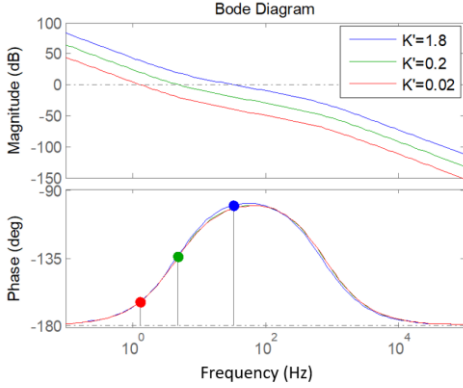


Fig. 8 Bode diagrams of bus voltage loop without BES compensation.

Put (1) into (5), T_{p2} can be obtained as,

$$T_{p2} = \frac{\tilde{v}_{PV}(s)}{\tilde{v}_{PV}(s)} = K_{PV}V_{PV} + I_{PV} = K' \quad (6)$$

where the gain K' is a constant depending on the PV operating point.

From (6), at steady state MPP operation,

$$\frac{d\tilde{v}_{PV}}{d\tilde{v}_{PV}} = K' = 0 \quad (7)$$

Fig. 6 shows the operation regions and relationships among PV parameters and PV curve. The unstable region yields the situation that $T_{p2} < 0$, which makes the overall system a positive feedback system.

By adding perturbation to v_{bus} energy balance equation,

$$\frac{c_{bus}}{2} \frac{d(v_{bus} + \tilde{v}_{bus})^2}{dt} = P_{bus} + \tilde{p}_{bus} \quad (8)$$

T_{p3} can be obtained as,

$$T_{p3} = \frac{\tilde{v}_{bus}(s)}{\tilde{p}_{bus}(s)} = \frac{1}{c_{bus}V_{bus}s} \quad (9)$$

When without BES HPF loop, $p_{bus} = p_{PV}$; when with BES HPF loop, $p_{bus} = p_{PV} + p_{BES}$.

Transfer functions of PI controllers for v_{bus} loop and v_{PV} loop can be expressed as,

$$T_{PI,bus} = \frac{\tilde{v}_{PV,ref}(s)}{\tilde{v}_{err}(s)} = \frac{k_{p,bus}s + k_{i,bus}}{s} \quad (10)$$

$$T_{PI,PV} = \frac{\tilde{i}_{PV,ref}(s)}{\tilde{v}_{PV}(s)} = -\frac{k_{p,PV}s + k_{i,PV}}{s} \quad (11)$$

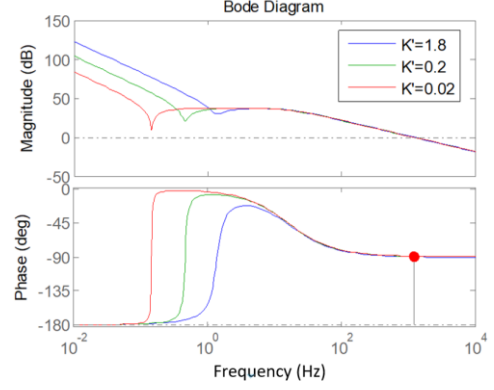


Fig. 9 Bode diagrams of bus voltage loop with BES HPF compensation.

The HPF in BES dynamic compensation loop can be written as,

$$T_{HPF} = \frac{t_{HPF}s}{t_{HPF}s + 1} \quad (12)$$

B. PV voltage loop

With (11) and (4), the v_{PV} loop open-loop transfer function can be obtained,

$$T_{OL,VPV} = T_{PI,PV} \cdot T_{p1} = \frac{k_{p,PV}s + k_{i,PV}}{-C_{PV}s^2 + K_{PV}s} \quad (13)$$

Assuming the PV current loop crossover frequency is around 4kHz (switching frequency is 20kHz). The crossover frequency of v_{PV} loop should be 5 times lesser at least, which is around 800 Hz. With parameters given in Table II, bode diagram of v_{PV} open-loop transfer function can be obtained as Fig. 7. With K_{PV} varying in the range of -0.01 to -0.1, the crossover frequency kept close to 717 Hz with a phase margin in the range of 88.5 to 94.2 degree. Thus, the PV voltage loop is robust towards PV parameters variation.

C. Dc bus voltage loop

1. Without BES compensation

The closed-loop transfer function between i_{PV} and $v_{PV,ref}$ can be derived as,

$$T_{CL,VPV} = \frac{T_{OL,VPV}}{1 + T_{OL,VPV}} \quad (14)$$

Without BES HPF loop, the v_{bus} open-loop transfer function is,

$$T_{OL,Vbus1} = T_{PI,bus} \cdot T_{CL,VPV} \cdot T_{p2} \cdot T_{p3} \quad (15)$$

The open loop gain of (15) can be derived as,

$$K_{OL,Vbus1} = \frac{k_{p,PV} \cdot k_{p,bus} \cdot K'}{C_{PV}C_{bus}V_{bus}} \quad (16)$$

Notice that K' may vary a lot due to different operation conditions of PV generation, which could affect the overall system performance. Especially when the operating point is close to MPP, K' will be close to zero and slows down the system response.

Fig. 8 shows bode diagrams of dc bus voltage loop with K' varying from 0.02 to 1.8. System crossover frequency is badly affected due to K' change. When K' is reduced, the control bandwidth decreases significantly (4.8 Hz when $K'=0.2$, 1.3 Hz when $K'=0.02$), with insufficient phase margins (45 degree when $K'=0.2$, 15.5 degree when $K'=0.02$).

Furthermore K' has to be positive to guarantee a positive loop gain. Thus, considering (7), it is necessary to keep PV generation operating in the range of $\frac{d\tilde{v}_{PV}}{d\tilde{v}_{PV}} > 0$. However, the output of MPPT controller changes very slow. To avoid operation in the unstable range, the saturator in PV controller, as shown in Fig. 2, limits the PV voltage to operate in the stable range. However, the V_{MPP} tracking is very slow, so the PV has a chance operating in the unstable range for a short time during transient, which could cause stability issues towards transient operations.

Thus, in generation-dominating mode, the voltage regulation solely relying on PV converter has relatively poor performance and less robustness. A compensation from other MG components is necessary to keep the bus voltage regulation under acceptable performance.

1. With BES compensation

As mentioned, a compensation from other MG components is necessary to keep a good bus voltage regulation performance. This can be achieved by using existing BESs. Though in generation-dominating mode, BES is saturated, it can still provide dynamic compensation which would not cause significant amount of energy flow.

As Fig. 4 (b) showing the control diagram, the v_{bus} open-loop transfer function is,

$$T_{OL,Vbus2} = (T_{PI,bus} \cdot T_{CL,VPV} \cdot T_{p2} + T_{HPF} \cdot m_2 \cdot V_{BAT}) \cdot T_{p3} \quad (17)$$

Fig. 9 shows bode plots of transfer function (17) with different PV parameters. It can be seen the crossover frequency stays constantly around 1200 Hz with phase margin around 90 degree towards K' variation. And the crossover frequency can be kept at a relatively high value despite the inner PV voltage loop restriction. Thus, the BES compensation loop, as a feed-forward loop, which is independent from PV parameters, can make the system more resistive towards PV parameter change and improve system's dynamic performance.

Thus, with BES compensation, even under generation-dominating mode, the dc bus voltage regulation can be kept robust and with a good dynamic performance.

D. Overall system analysis using state space model

To evaluate the performance of overall system involving the V-I droop control, the transfer function method would become too complicated due to the droop controller has an interaction with the inner loop output p_{bus} . Thus, a state space model is provided for overall system evaluation.

The closed-loop state equations for the system can be expressed as,

$$\dot{X} = A \cdot X + B \cdot U \quad (18)$$

For system given in Fig. 5 (a), the state vector can be selected as,

$$X_1 = [\tilde{v}_{bus} \quad \tilde{v}_{PV} \quad \tilde{v}_{PV,ref} \quad \tilde{i}_{PV}]^T \quad (19)$$

The differential equations for each state variable can be obtained by applying Inverse Laplace Transform to the transfer functions.

From (6) and (9), the differential equation of \tilde{v}_{bus} is,

$$\frac{d\tilde{v}_{bus}}{dt} = \frac{\tilde{p}_{bus}}{C_{bus}V_{bus}} = \frac{K'}{C_{bus}V_{bus}} \tilde{v}_{PV} \quad (20)$$

From (4), the differential equation of \tilde{v}_{PV} is,

$$\frac{d\tilde{v}_{PV}}{dt} = \frac{K_{PV}}{C_{PV}} \tilde{v}_{PV} - \frac{1}{C_{PV}} \tilde{i}_{PV} \quad (21)$$

From (10), the differential equation of $\tilde{v}_{PV,ref}$ is,

$$\frac{d\tilde{v}_{PV,ref}}{dt} = k_{p,bus} \left(rK' \frac{d\tilde{v}_{PV}}{dt} - \frac{d\tilde{v}_{bus}}{dt} \right) + k_{i,bus} (rK' \tilde{v}_{PV} - \tilde{v}_{bus}) \quad (22)$$

From (11), the differential equation of \tilde{i}_{PV} is,

$$\frac{d\tilde{i}_{PV}}{dt} = -k_{p,PV} \left(\frac{d\tilde{v}_{PV,ref}}{dt} - \frac{d\tilde{v}_{PV}}{dt} \right) - k_{i,PV} (\tilde{v}_{PV,ref} - \tilde{v}_{PV}) \quad (23)$$

From (20)-(23), the system matrix A_1 can be written as follow,

$$A_1 = \begin{bmatrix} 0 & \frac{K'}{C_{bus}V_{bus}} & 0 & 0 \\ 0 & \frac{K_{PV}}{C_{PV}} & 0 & -\frac{1}{C_{PV}} \\ -k_{i,bus} & a_{32} & 0 & -\frac{rK'k_{p,bus}}{C_{PV}} \\ k_{p,pv}k_{i,bus} & a_{42} & -k_{i,pv} & a_{44} \end{bmatrix} \quad (24)$$

where

$$a_{32} = -\frac{rK'k_{p,bus}k_{p,pv}}{C_{PV}} + rK'k_{i,bus} - \frac{k_{p,bus}K'}{C_{bus}V_{bus}}$$

$$a_{42} = -k_{p,pv} \cdot a_{32} + \frac{k_{p,pv}K_{PV}}{C_{PV}} + k_{i,pv}$$

$$a_{44} = \frac{k_{p,pv}(1 - rK'k_{p,bus})}{C_{PV}}$$

For system given in Fig. 5 (b), the state vector is selected as,

$$X_2 = [\tilde{v}_{bus} \quad \tilde{v}_{PV} \quad \tilde{v}_{PV,ref} \quad \tilde{i}_{PV} \quad \tilde{z}]^T \quad (25)$$

Follow the similar approach, the system matrix A_2 is,

$$A_2 = \begin{bmatrix} 0 & \frac{K'}{C_{bus}V_{bus}} & 0 & 0 & \frac{mV_{bat}}{C_{bus}V_{bus}} \\ 0 & \frac{K_{PV}}{C_{PV}} & 0 & -\frac{1}{C_{PV}} & 0 \\ -k_{i,bus} & a_{32} & 0 & -\frac{rK'k_{p,bus}}{C_{PV}} & 0 \\ k_{p,pv}k_{i,bus} & a_{42} & -k_{i,pv} & a_{44} & 0 \\ 0 & -\frac{K'}{C_{bus}V_{bus}} & 0 & 0 & -\frac{1}{t_{HPF}} \end{bmatrix} \quad (26)$$

where a_{32}, a_{42}, a_{44} are same as provided in (24).

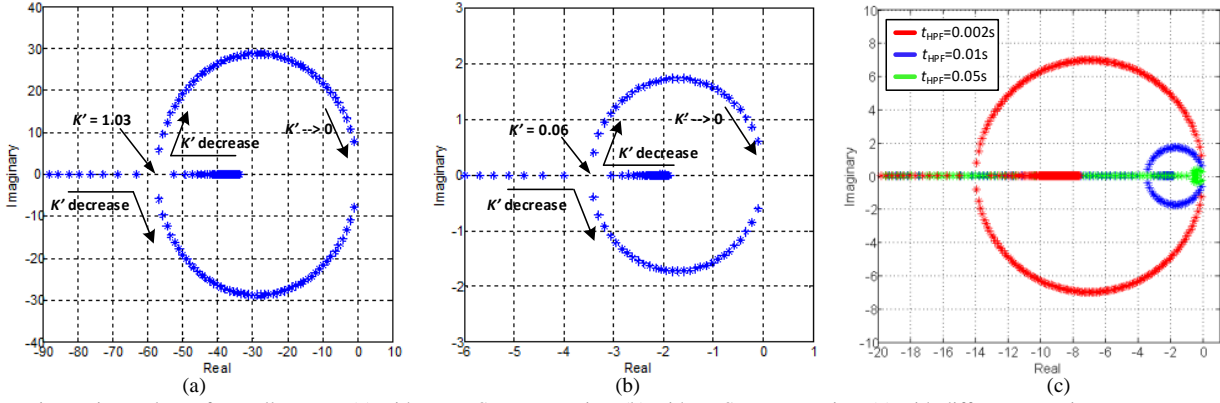


Fig. 10 Dominant eigenvalues of overall system, (a) without BES compensation, (b) with BES compensation, (c) with different HPF time constants.

1. Without BES compensation

To simplify the analysis of a high-order system, the dominant eigenvalue approximation can be applied when the other eigenvalues are much further from the imaginary axis than the dominant poles.

With state matrix given by (24), Fig. 10 (a) shows changes of dominant eigenvalues along with PV operating point change. It can be seen the system is stable as long as $K' > 0$. However, when $K' < 1.03$, the dominant eigenvalues become a pair of conjugate eigenvalues with relatively large imaginary parts, which could lead to significant oscillation during dynamic process.

2. With BES compensation

With state matrix given by (26), Fig. 10 (b) shows changes of dominant eigenvalues along with PV operating point change. The system is stable as long as $K' > 0$. And, when $K' < 0.06$, the dominant eigenvalues become a pair of conjugate eigenvalues with small imaginary parts ($\omega < 1.7$ rad/s).

The system with BES compensation is less likely being oscillated: only when $K' < 0.06$ (almost on the MPP point), dominant eigenvalues become conjugate; oscillating frequency is very low that $\omega < 1.7$ rad/s.

However, involvement of BES compensation pushes dominant eigenvalues closer to imaginary axis due to the HPF. As a result, the dynamic response will be slowed down inevitably.

Fig. 10 (c) shows the loci with different t_{HPF} . Obviously, there is a trade-off between oscillation and dynamic response speed. In this case of dc bus voltage regulation, slow dynamic response speed is acceptable that the dc bus voltage should not have big step changes during normal operation, which will be discussed in simulation study.

IV. SIMULATION AND EXPERIMENTAL STUDY

A. Simulation Study

Simulations based on PLECS are performed to verify the analytical study. Table II shows parameters used in simulation. To validate the analytical study, one of the worst scenarios that PV changes from MPPT control to bus voltage droop control at light load is tested in simulation and experiment study.

Simulation results of PV-BES droop control coordination without BES HPF compensation are shown in Fig. 11. At the

transient, BES gets fully charged and PV converter takes over bus voltage droop control. It can be seen in Fig. 11 (a), at 25W load, the bus voltage has a 14% overshoot at the transient of PV changing to droop control. With lighter load, in Fig. 11 (b), the overshoot is increased to 20%, which has been far beyond acceptable voltage fluctuation range. With higher PV generation rating or less loads, the voltage spike could even be further increased.

Simulation results of PV-BES droop control coordination with BES HPF compensation are shown in Fig. 12. In Fig. 12 (a), at 25W load, the bus voltage only has a 4.8% overshoot at the transient of PV shifting to droop control. At 2.5W load, in Fig. 12 (b), the overshoot is still kept around 4.7%. Though it requires much longer time to settle down as proved by loci in Fig. 10, the bus voltage is always kept inside a very small fluctuation range, which has neglectable effect to the MG system. With BES HPF compensation, BES power is not saturated to zero immediately at the transient, it slowly reaches zero which prevent bus voltage from ramping up.

Fig. 13 shows simulation result of two PV units and two BES units operating in parallel with proposed PV-BES coordination control. In t_0 - t_1 , both PVs operate under MPPT (with different MPP powers); bus voltage is regulated by both BES units. At t_1 , BES1 is fully charged while BES2 can still absorb surplus power. Hence in t_1 - t_2 both PVs still work under MPPT and bus voltage is regulated solely by BES2. At t_2 , BES2 also gets fully charged, PVs take over bus voltage regulation. With BES HPF compensation, the transient process is smooth with very small overshoot, and the compensated energy from BESs are equally shared by BES1 and BES2. At t_3 , solar irradiance on PV1 is stepped up. With BES compensation, dc bus voltage only has a very small fluctuation towards irradiance change. At t_4 , load is reduced from 30W to 5W, the voltage transient is again kept smooth with BES compensation.

B. Experiment Verification

The proposed PV-BES coordination control has been verified by laboratory experiment with one PV unit and one BES unit, of which the setup is shown in Fig. 14. A PV simulator is used to emulate PV behavior. Converters are controlled by a TI F28379d DSP. Parameters are set same as Table II. Fig. 15 shows experimental results of PV-BES coordination control transient with different BES HPF time

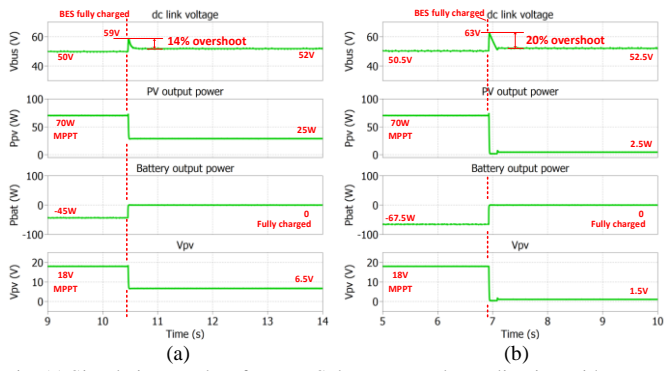


Fig. 11 Simulation results of PV-BES droop control coordination without BES HPF compensation, (a) with 25W load, (b) with 2.5W load.

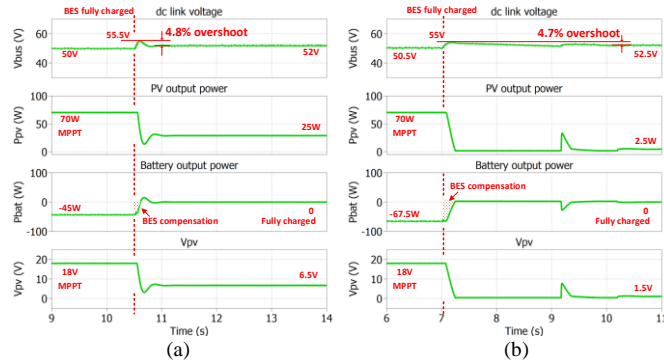


Fig. 12 Simulation results of PV-BES droop control coordination with BES HPF compensation, (a) with 25W load, (b) with 2.5W load.

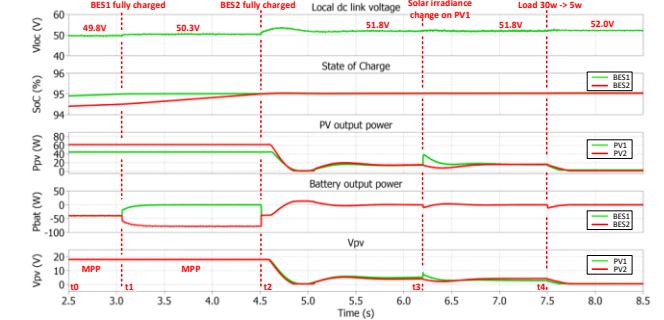


Fig. 13 Simulation results of power sharing with proposed PV-BES coordination control, with two PV units and two BES units.

constants. In Fig. 15 (a), BES HPF is inactive or $t_{HPF} = 0$. The transient of PV changing to droop control causes a large overshoot on dc bus voltage, which agrees to simulation result in Fig. 11 (a). In Fig. 15 (b), t_{HPF} is increased to 0.01. With help of BES HPF compensation, the transient becomes much smoother with a 3V overshoot. In Fig. 15 (c), t_{HPF} is further increased to 0.05, and the transient overshoot is further damped to around 2V, which agrees to simulation result Fig. 12 (a).

With proposed BES HPF compensation loop, even under very light load condition, the PV voltage regulation can be kept at a good performance. Fig. 16 shows the experimental result that PV changing to droop control with 2.5W load. The overshoot is kept around 2V and the waveforms show a good agreement to simulation result Fig. 12 (b).

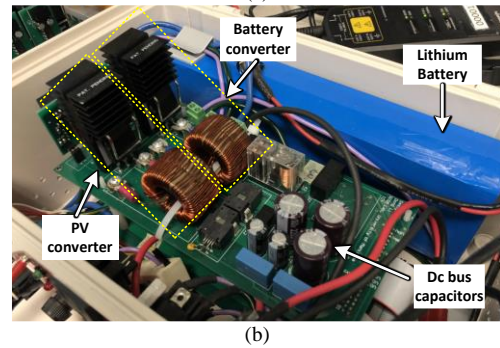
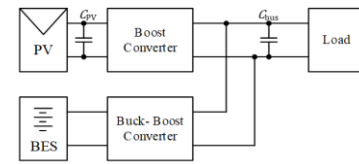


Fig. 14 Experiment setup, (a) connection diagram, (b) photo.

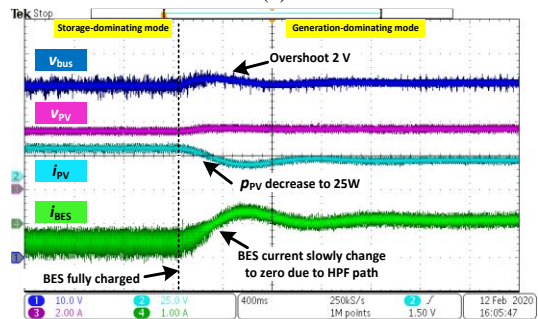
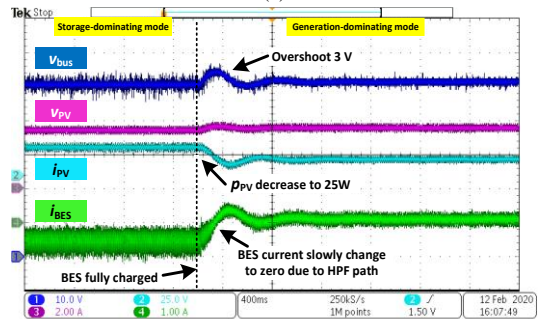
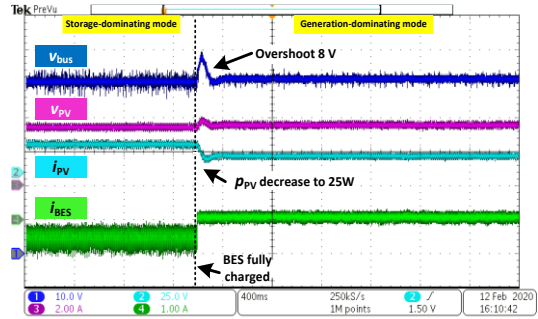


Fig. 15 Experimental results of PV-BES coordination control, at transient of PV taking over bus voltage control and load is at 25W, (a) without BES HPF compensation, (b) with BES HPF compensation and $t_{HPF} = 0.01$, (c) with BES HPF compensation and $t_{HPF} = 0.05$.

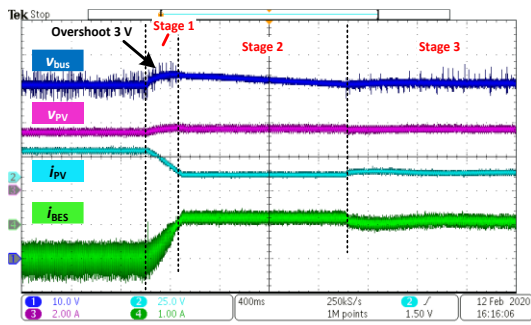


Fig. 16 Experimental result of PV-BES coordination control, at transient of PV taking over bus voltage control and load is at 2.5W, with BES HPF compensation and $t_{HPF} = 0.05$.

It can be observed from all the results, that the transient has three stages (it is more obvious in Fig. 16 due to the longer settling time). In the first stage, BES gets fully charged, bus voltage raises up, BES charging current decreases slowly due to the HPF path which keeps bus voltage from overshooting too much. In the second stage, PV output power has reduced lower than load, bus voltage decreases. The HPF path will always obstruct bus voltage change. As a result, BES will discharge in this stage. In the third stage, bus voltage reduces to the value set by droop controller; output of BES HPF settles to zero, and new steady state is reached.

Fig. 17 shows experimental results when two BES units are connected to the same dc bus. From Fig. 17 (a), it can be seen, the system is under storage-dominating mode as long as one of the BES units could regulate the dc bus voltage. At the transient of BES2 gets fully charged, both BES units can provide dynamic compensation, and the dynamic compensation current can be equally shared among the BES units. The transient bus voltage is smooth and with a very small overshoot. Fig. 17 (b) shows the dynamic compensation from BES units when under generation-dominating mode. When solar irradiance has a sudden change, both BES units can provide dynamic compensation temporarily despite the SoC limit. Fig. 17 (c) shows the transient that when PV output power cannot supply load, BES units start to discharge, and the system is under storage-dominating mode.

V. CONCLUSIONS

In this paper, a PV-BES coordination control method is proposed to overcome the control issue of bus voltage regulation under PV-dominating mode. The whole control scheme is kept in a decentralized and communication-less manner, which can be used for Plug-n-Play (PnP) microgrid. The proposed method utilizes existing BES systems. With decoupled control loops, BESs can still provide dynamic compensation even under generation-dominating mode. The proposed control method has been analyzed with small signal analysis and verified by both simulation and experimental result.

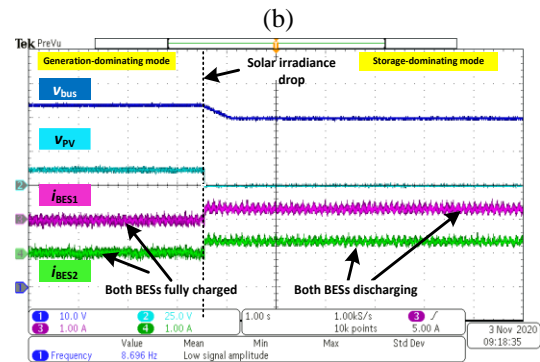
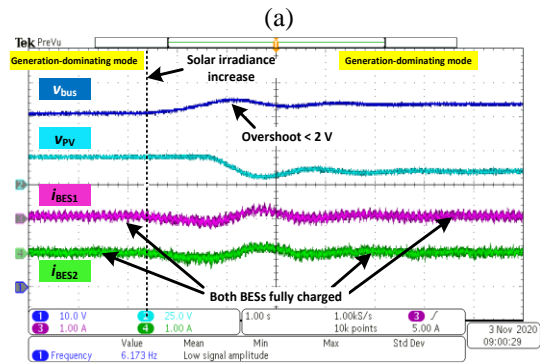
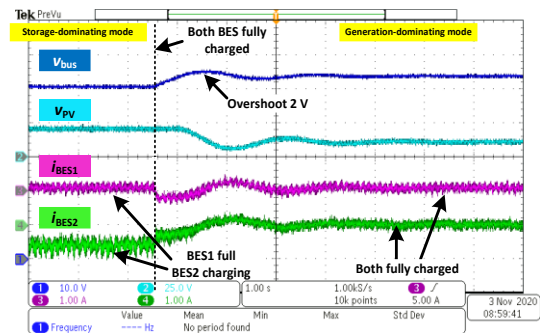


Fig. 17 Experimental result of PV-BES coordination control, with two BES modules operate in parallel, with load of at 25W and BES HPF compensation and $t_{HPF} = 0.05$: (a) transient waveforms of BES1 full & BES2 charging to BES1 full & BES2 full; (b) transient waveforms of solar irradiance step increase when both BESs are fully charged; (c) transient waveforms of solar irradiance drop to zero and operation mode change to storage-dominating mode.

REFERENCES

- [1] M. Nasir, H. A. Khan, N. A. Zaffar, J. C. Vasquez and J. M. Guerrero, "Scalable Solar dc Micrigrids: On the Path to Revolutionizing the Electrification Architecture of Developing Communities," *IEEE Electric. Mag.*, vol. 6, no. 4, pp. 63-72, Dec. 2018.
- [2] D. Li, C. N. M. Ho and K. K. M. Siu, "A Method for Solving Current Unbalance Problem of Paralleled Single-Phase Grid-Connected Unipolar-PWM Inverters With Common Dc Bus," *IEEE Trans. Ind. Appl.*, vol. 55, no. 6, pp. 7595-7603, Nov.-Dec. 2019.
- [3] K. Yan, Y. Du and Z. Ren, "MPPT Perturbation Optimization of Photovoltaic Power Systems Based on Solar Irradiance Data Classification," *IEEE Trans. Sustain. Energy*, vol. 10, no. 2, pp. 514-521, April 2019.
- [4] V. T. Dragičević, X. Lu, J. C. Vasquez and J. M. Guerrero, "DC Microgrids—Part I: A Review of Control Strategies and Stabilization Techniques," *IEEE Trans. Power Electron.*, vol. 31, no. 7, pp. 4876-4891, July 2016.

- [5] H. Kakigano, Y. Miura and T. Ise, "Distribution Voltage Control for DC Microgrids Using Fuzzy Control and Gain-Scheduling Technique," *IEEE Trans. Power Electron.*, vol. 28, no. 5, pp. 2246-2258, May 2013.
- [6] A. P. N. Tahim, D. J. Pagano, E. Lenz and V. Stramosk, "Modeling and Stability Analysis of Islanded DC Microgrids Under Droop Control," *IEEE Trans. Power Electron.*, vol. 30, no. 8, pp. 4597-4607, Aug. 2015.
- [7] A. Werth, N. Kitamura and K. Tanaka, "Conceptual Study for Open Energy Systems: Distributed Energy Network Using Interconnected DC Nanogrids," *IEEE Trans. Smart Grid*, vol. 6, no. 4, pp. 1621-1630, July 2015.
- [8] L. Meng et al., "Review on Control of DC Microgrids and Multiple Microgrid Clusters," in *IEEE J. Emerg. Sel. Topics Power Electron.*, vol. 5, no. 3, pp. 928-948, Sept. 2017.
- [9] P. A. Madduri, J. Poon, J. Rosa, M. Podolsky, E. A. Brewer and S. R. Sanders, "Scalable DC Microgrids for Rural Electrification in Emerging Regions," *IEEE J. Emerg. Sel. Topics Power Electron.*, vol. 4, no. 4, pp. 1195-1205, Dec. 2016.
- [10] S. Liptak, M. Miranbeigi, S. Kulkarni, R. Jinsiwale and D. Divan, "Self-Organizing NanoGrid (SONG)," *2019 IEEE Decentralized Energy Access Solutions Workshop (DEAS)*, Atlanta, GA, USA, 2019, pp. 206-212.
- [11] M. Nasir, Z. Jin, H. A. Khan, N. A. Zaffar, J. C. Vasquez and J. M. Guerrero, "A Decentralized Control Architecture Applied to DC Nanogrid Clusters for Rural Electrification in Developing Regions," *IEEE Trans. Power Electron.*, vol. 34, no. 2, pp. 1773-1785, Feb. 2019.
- [12] V. Nasirian, S. Moayedi, A. Davoudi and F. L. Lewis, "Distributed Cooperative Control of DC Microgrids," *IEEE Trans. Power Electron.*, vol. 30, no. 4, pp. 2288-2303, April 2015.
- [13] M. B. Shadmand, R. S. Balog and H. Abu-Rub, "Model Predictive Control of PV Sources in a Smart DC Distribution System: Maximum Power Point Tracking and Droop Control," *IEEE Trans. Energy Convers.*, vol. 29, no. 4, pp. 913-921, Dec. 2014.
- [14] Y. Gu, X. Xiang, W. Li and X. He, "Mode-Adaptive Decentralized Control for Renewable DC Microgrid With Enhanced Reliability and Flexibility," *IEEE Trans. Power Electron.*, vol. 29, no. 9, pp. 5072-5080, Sept. 2014.
- [15] D. Li and C. N. M. Ho, "A Module-Based Plug-n-Play Dc Microgrid with Fully Decentralized Control for IEEE Empower a Billion Lives Competition," *IEEE Trans. Power Electron.*, vol. 36, no. 2, pp. 1764-1776, Feb. 2021, doi: 10.1109/TPEL.2020.3009631.
- [16] X. Lu, K. Sun, J. M. Guerrero, J. C. Vasquez and L. Huang, "Double-Quadrant State-of-Charge-Based Droop Control Method for Distributed Energy Storage Systems in Autonomous DC Microgrids," *IEEE Trans. Smart Grid*, vol. 6, no. 1, pp. 147-157, Jan. 2015.
- [17] A. Elrayah, Y. Sozer and M. E. Elbuluk, "Modeling and Control Design of Microgrid-Connected PV-Based Sources," *IEEE J. Emerg. Sel. Topics Power Electron.*, vol. 2, no. 4, pp. 907-919, Dec. 2014.
- [18] H. Cai, J. Xiang and W. Wei, "Decentralized Coordination Control of Multiple Photovoltaic Sources for DC Bus Voltage Regulating and Power Sharing," *IEEE Trans. Ind. Electron.*, vol. 65, no. 7, pp. 5601-5610, July 2018.
- [19] Q. Xu et al., "A Decentralized Dynamic Power Sharing Strategy for Hybrid Energy Storage System in Autonomous DC Microgrid," *IEEE Trans. Ind. Electron.*, vol. 64, no. 7, pp. 5930-5941, July 2017.
- [20] H. Wang, M. Han, R. Han, J. M. Guerrero and J. C. Vasquez, "A Decentralized Current-Sharing Controller Endows Fast Transient Response to Parallel DC-DC Converters," *IEEE Trans. Power Electron.*, vol. 33, no. 5, pp. 4362-4372, May 2018.
- [21] X. Lu, K. Sun, J. M. Guerrero, J. C. Vasquez and L. Huang, "State-of-Charge Balance Using Adaptive Droop Control for Distributed Energy Storage Systems in DC Microgrid Applications," *IEEE Trans. Ind. Electron.*, vol. 61, no. 6, pp. 2804-2815, June 2014.
- [22] H. Cai, J. Xiang and W. Wei, "Modelling, analysis and control design of a two-stage photovoltaic generation system," in *IET Renewable Power Generation*, vol. 10, no. 8, pp. 1195-1203, 9 2016.
- [23] J. A. Gow and C. D. Manning, "Development of a photovoltaic array model for use in power-electronics simulation studies," in *IEE Proceedings - Electric Power Applications*, vol. 146, no. 2, pp. 193-200, March 1999.